Anyonic topological flat bands

3 authors, including:

Xiaoqi Zhou
Beijing Institute of Technology
5 PUBLICATIONS   **11** CITATIONS

SEE PROFILE

Weixuan Zhang
Beijing Institute of Technology
112 PUBLICATIONS   **2,212** CITATIONS

SEE PROFILE

Anyonic topological flat bands

Xiaoqi Zhou, Weixuan Zhang[†], Xiangdong Zhang[‡]

Key Laboratory of advanced optoelectronic quantum architecture and measurements of Ministry of Education,

Beijing Key Laboratory of Nanophotonics & Ultrafine Optoelectronic Systems, School of Physics,

Beijing Institute of Technology, Beijing 100081, China

Corresponding authors. E-mail: [†]zhangwx@bit.edu.cn, [‡]zhangxd@bit.edu.cn

ABSTRACT

Topological flat bands have attracted significant interest across various branches of physics, where synthetic gauge fields are typically considered an essential prerequisite. Numerous mechanisms have been proposed for implementing these fields, including magnetic fields on electrons, differential optical paths for photons, and strain-induced effective magnetic fields, among others. In this work, we introduce a novel approach to generating synthetic gauge fields through quantum statistics and demonstrate their effectiveness in realizing anyonic topological flat bands. Notably, we discover that a pair of strongly interacting anyons can induce square-root topological flat bands within a lattice model that remains dispersive and topologically trivial for a single particle. To validate our theoretical predictions, we experimentally simulate the quantum statistics-induced topological flat bands and square-root topological boundary states by mapping the eigenstates of two anyons onto modes in electric circuits. Our findings not only open a new pathway for creating topological flat bands but also deepen our understanding of anyonic physics and the underlying principles of flat-band topology.
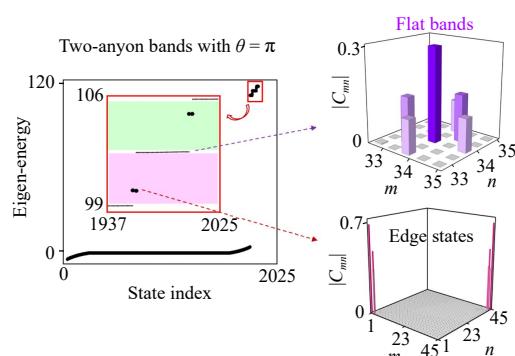
1 Introduction

In recent decades, flat bands with exotic topological properties have garnered significant attention across various disciplines, including condensed matter physics and artificial quantum and classical systems [1–8]. A pioneering example is the two-dimensional (2D) electron gas subjected to a perpendicular magnetic field, where Landau levels with non-zero Chern numbers emerge [9]. More recently, the study of complete topological flat bands in discrete lattices has sparked considerable interest. One established approach to achieving complete flat bands in electronic lattices involves introducing magnetic flux with specific values, where destructive interference among different propagation paths leads to

the formation of compact localized states known as Aharonov–Bohm (AB) cages [10–14]. Although initially applied to electronic systems, it has since been recognized that synthetic magnetic fields can extend this phenomenon to non-electronic lattices [15–21], creating opportunities to observe complete topological flat bands in various artificial bosonic and classical-wave systems.

Motivated by the distinctive features of flux-controlled flat-band localization, extensive investigations have also been conducted on the influence of particle interactions within AB cages [22–32]. Preliminary studies have shown that these interactions can cause delocalization in fully flat-band systems [22, 23], a phenomenon that has indeed been experimentally observed [24]. More recently, it has been noted that strong interaction effects
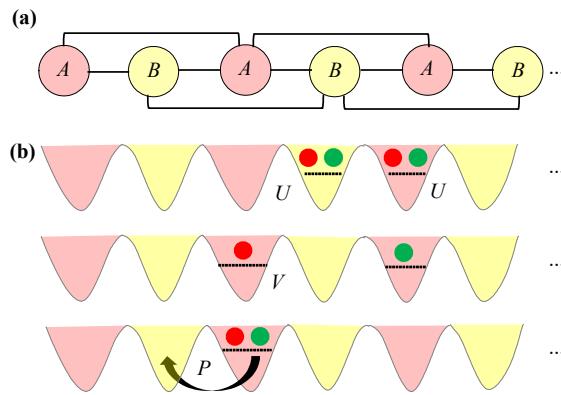
can lead to the formation of doublons from two bosonic particles, which themselves exhibit AB caging behavior under half-valued flux conditions [27–30]. Furthermore, non-trivial topological edge states have been observed within these doublon-based AB cages [30]. All existing proposals for topological flat bands within single- and few-particle AB cages require complex-valued single-particle hoppings induced by synthetic gauge flux to achieve destructive interference.

In this work, we demonstrate that flat bands with non-trivial topology can be induced purely by quantum statistics in a one-dimensional (1D) two-anyon lattice model. Anyons, predicted in the 1980s, are quantum particles or excitations with exchange statistics that are intermediate between bosons and fermions [33–52]. Previous studies have shown that quantum statistics can induce various novel effects, such as anyonic Bloch oscillations [47, 48], anyonic bound states in the continuum [49], and quantum statistics-induced topological transitions [50]. Despite these advances, quantum statistics has never before been shown to act as synthetic gauge flux and trigger the formation of non-trivial flat-band topology. Here, we reveal that two-anyon flat bands associated with square-root topology can be purely induced by quantum statistics. Moreover, by mapping two-anyon states in a one-dimensional lattice to the modes of a two-dimensional circuit network, we experimentally simulate the anyonic flat-band localizations and square-root topological boundary states. Our results open the door to novel physics arising from the interplay between strong interactions and anyonic correlations, and suggest a new route to simulating effective magnetic fields through quantum statistics.

2 The theory of quantum statistics-induced anyonic topological flat bands

We consider a pair of interacting anyons hopping on a 1D chain with N units, and each unit contains two sublattices marked by "A" and "B". Figure 1(a) illustrates the nearest neighbor (NN) and next-nearest neighbor (NNN) hoppings (J) and Fig. 1(b) presents three types of two-anyon interactions, including the on-site interaction at both sublattices (U), NN interaction at "A" sublattice (V), and direct two-anyon hopping (P). The model can be described by the extended anyon-Hubbard Hamiltonian as
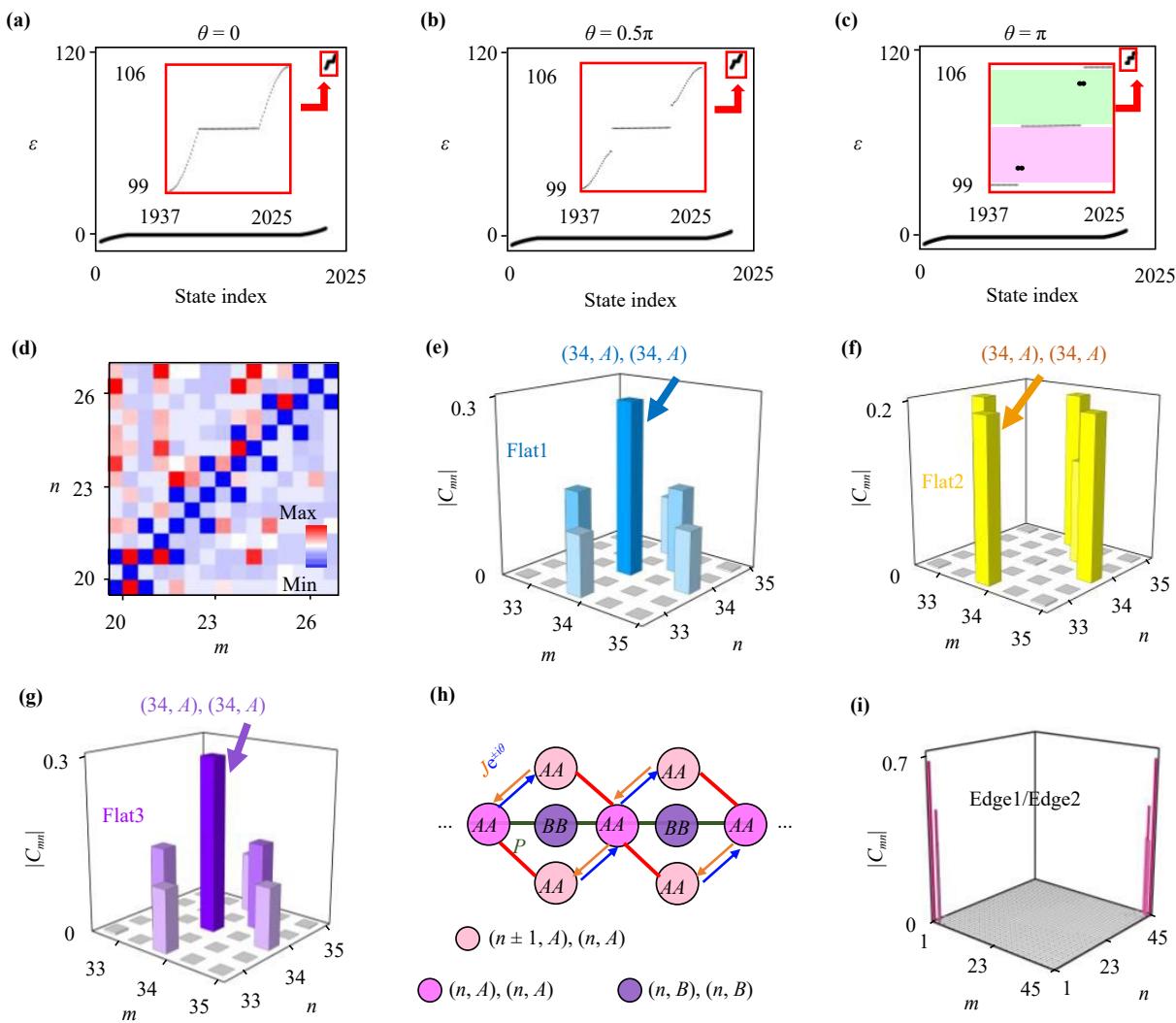
$$
\begin{aligned}
H = \sum_{l=1}^{N} [&-J(a_{l,A}^+ a_{l,B} + a_{l,B}^+ a_{l+1,A} + a_{l,A}^+ a_{l+1,A} \\
&+ a_{l,B}^+ a_{l+1,B}) - 0.5P(a_{l,A}^+ a_{l,A}^+ a_{l,B} a_{l,B} \\
&+ a_{l,B}^+ a_{l,B}^+ a_{l+1,A} a_{l+1,A}) + 0.5U n_{l,A}(n_{l,A}-1) \\
&+ 0.5U n_{l,B}(n_{l,B}-1) + V n_{l,A} n_{l+1,A}] + h.c.,
\end{aligned}
$$

(1)

Fig. 1 The theoretical model of two-anyon systems sustaining quantum statistics-induced completely topological flat bands. **(a)** The schematic diagram for the 1D single-particle lattice model with two types of sublattices. Each unit contains two sublattices marked by "A" and "B". The NN and NNN hoppings (J) are marked by black lines. **(b)** The schematic diagram of three types of two-anyon interaction effects, including the on-site interaction at both sublattices (U), the nearest-neighbor interaction at sublattice "A" (V), and the direct two-anyon hopping (P).

where $a_l^+(a_l)$ and $n_l = a_l^+ a_l$ are the creation (annihilation) operator and the particle number operator. The anyonic commutation relations are expressed as $\hat{a}_k^+ \hat{a}_l - \hat{a}_l^+ \hat{a}_k e^{i\theta sgn(l-k)} = \delta_{lk}$ and $\hat{a}_l \hat{a}_k - \hat{a}_k \hat{a}_l e^{i\theta sgn(l-k)} = 0$, where θ is the statistical angle. The two-anyon state can be expanded as $|\psi\rangle = \frac{1}{\sqrt{2}} \sum_{m,n=1}^{N} \sum_{\alpha,\beta \propto A,B} C_{(m,\alpha)(n,\beta)} a_{(m,\alpha)}^+ a_{(n,\beta)}^+ |0\rangle$, where $C_{(m,\alpha)(n,\beta)}$ is the probability amplitude with one anyon at "α" sublattice in the mth unit and the other one at "β" sublattice in the nth unit. By solving the steady-state Schrödinger equation, the eigen-equation of two-anyon state $C_{(m,\alpha)(n,\beta)}$ can be obtained (See Supplementary Note 1 for the detailed derivation).

The calculated eigenspectra of two anyons with the statistical angle being $\theta = 0$, 0.5π and π are shown in Figs. 2(a)–(c). Other parameters are set as $J = 1$, $P = \sqrt{2}$, $U = V = 100 + 2\sqrt{2}$, and $N = 45$. It is shown that two-anyon eigenspectra are separated by an energy gap ($\approx U$, V). The low-energy section ($\varepsilon \sim 0$) corresponds to scattering states of two anyons. The spatial profile of a two-anyon scattering state is depicted in Fig. 2(d), which is extended into lots of two-anyon states at non-diagonal positions in the Fock space. Zero amplitudes of $C_{(n,A)(n,A)}$, $C_{(n+1,A)(n,A)}$, $C_{(n,A)(n+1,A)}$, and $C_{(n,B)(n,B)}$ indicate that two anyons are always separated from each other in the low-energy region. High-energy eigenmodes ($\varepsilon \sim U, V$) correspond to two-anyon states with strong interactions. Enlarged views of high-energy eigenspectra are shown in three insets enclosed by red blocks. We can see that the statistical angle can significantly alter the dispersion of two-anyon bands with strong interactions. Specifically, when the statistical angle equals to zero, the

024205-2

Xiaoqi Zhou, et al., Front. Phys. 20(2), 024205 (2025)

Fig. 2 Numerical results of quantum statistics-induced two-anyon topological flat bands. **(a–c)** The calculated eigenspectra of two anyons with the statistical angle being $\theta = 0$, 0.5π and π. Other parameters are set as $J = 1$, $P = \sqrt{2}$, $U = V = 100 + 2\sqrt{2}$, and $N = 45$. The low-energy section ($\varepsilon \sim 0$) corresponds to scattering states of two anyons. Insets display the high-energy eigenspectra. **(d)** The spatial profile for the two-anyon scattering state. **(e–g)** Spatial profiles of two-pseudofermion flat bands at $\varepsilon = 100$, 102.8 and 105.7. The flat-band eigenmode at $\varepsilon = 102.8$ possesses the zero-value amplitude of $C_{(n,A)(n,A)}$. Other two flatbands have the large amplitude of $C_{(n,A)(n,A)}$. **(h)** The 1D effective model of two anyons with strong interactions. The unit is composed of four two-anyon states of $C_{(n,A)(n,A)}$, $C_{(n+1,A)(n,A)}$, $C_{(n,A)(n+1,A)}$, and $C_{(n,B)(n,B)}$. **(i)** The spatial profile of the midgap topological state for two anyons with strong interaction.

two-anyon flat band appears at $\varepsilon = 102.8$ and contact with other two dispersive bands. By increasing the anyonic statistical angle to $\theta = 0.5\pi$, the flat band with $\varepsilon = 102.8$ is separated from other bands. Interestingly, three nearly flat bands appear when the statistical angle equals to $\theta = \pi$ (pseudofermions). Figures 2(e)–(g) display compact localized states of three flatbands at $\varepsilon = 100$, 102.8 and 105.7. It is shown that the flat-band eigenmode at $\varepsilon = 102.8$ possesses the zero-value amplitude of $C_{(n,A)(n,A)}$. Other two flatbands have the large amplitude of $C_{(n,A)(n,A)}$. In Supplementary Note 2, we calculate energy spectra of the two-anyon model with different interaction strengths. It is found that the flatness of two-pseudofermion band is enhanced with the interaction

strength being increased.

The origin of two-anyon flat bands can be clarified with an analytic formula. It is noted that the coupling between two-anyon states with strong interactions and two-anyon scattering states is very weak. The behavior of two anyons in the original 1D lattice can be effectively simulated by a single particle in the mapped 2D lattice. In addition, the on-site interaction and NN interaction at sublattice "A" can be re-interpreted as the on-site potential of the mapped 2D lattice at the main diagonal and two lateral diagonals, respectively. Under strong interactions, the coupling between lattice sites with low- and high-valued on-site potentials can be neglected, allowing the lattice sites with high-valued on-site potentials

can be treated as an 1D effective model. In this case, the effective model of two anyons with strong interactions can be viewed as a 1D superlattice, as shown in Fig. 2(h). The unit of the 1D effective lattice is composed of four two-anyon states of $C_{(n,A)(n,A)}$, $C_{(n+1,A)(n,A)}$, $C_{(n,A)(n+1,A)}$, and $C_{(n,B)(n,B)}$, with the effective Hamiltonian in the momentum space being expressed as

$$H(k)$$
$$= \begin{pmatrix} 0 & Je^{ik} + Je^{i\theta} & Pe^{ik} + P & Je^{ik} + J \\ Je^{-ik} + Je^{-i\theta} & 0 & 0 & 0 \\ Pe^{-ik} + P & 0 & 0 & 0 \\ Je^{-ik} + J & 0 & 0 & 0 \end{pmatrix}.$$
(2)
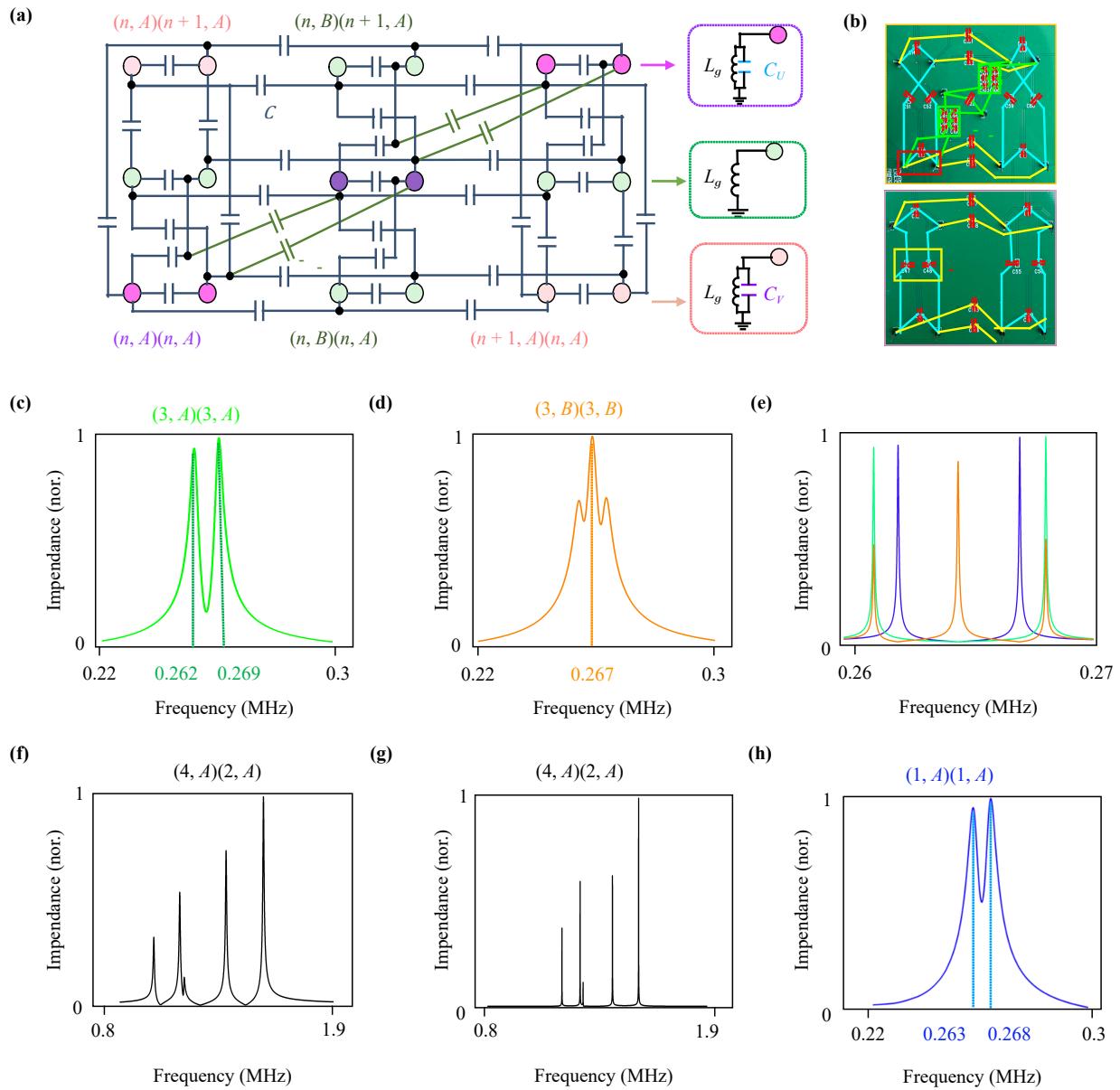
Four Bloch bands $E_{1,2,3,4}(k)$ can be solved as $E_{1,4}(k) = \pm(4J^2\cos k\cos\theta + 2P^2\cos k + 4J^2 + 2P^2)^{1/2}$ and $E_{2,3}(k) = 0$. We can see that the complete two-anyon flat bands can appear in the strong-interaction region when the statistical angle and hopping strengths satisfy $2J^2\cos\theta + P^2 = 0$. In this case, we can see that system parameters ($J = 1$ and $P = \sqrt{2}$) used in the two-pseudofermion model with nearly flat bands satisfy this formula. It is worth noting that the effective two-anyon model possesses a similar caging condition to that of a single-particle AB caging with two synthetic gauge fluxes in each unit [56]. In Supplementary Note 3, we provide numerical results on the generation of anyonic flat bands with other statistical angles. These results are consistent with the analytical prediction. It is worth noting that the emergence of anyonic flat bands in our model differs significantly from previous studies that rely on complex hoppings of a single particle or multiple particles. Our model only involves real-valued lattice hoppings, where the synthetic gauge flux arises from the statistical phase resulting from the exchange of two anyons. In this scenario, the statistical correlation effectively acts as an effective magnetic field, leading to the appearance of anyonic flat bands. It is worth noting that the appearance of the two-anyon flat bands is not coincidental but rather a consequence of the specific design of single-particle and two-anyon hopping strengths as well as the two-anyon interactions.

In addition, quantum statistics can also generate the topological edge mode in bandgaps between anyonic flatbands, as shown in Fig. 2(c). Figure 2(i) presents the corresponding spatial profile, manifesting the appearance of topological edge states of two strongly interacting anyons. To further illustrate the topological origin of anyonic midgap edge states, we compute the topological invariant in 1D momentum space of the two-anyon effective Hamiltonian. We focus on the case with $\theta = \pi$, where a two-fold degenerated zero-energy band and other two isolated flat-bands exist. The Zak's phase $\gamma_{iso} = i\int_\pi^{-\pi} Pdk\langle\nu_i(k)|\partial_k|\nu_i(k)\rangle$ ($i = 1, 4$) of each isolated

flat band ($|\nu_i(k)>$ is the eigenmode) is calculated. As for the degenerated zero-energy band, we use the Wilzcek–Zee phase $\gamma_d = \int_\pi^{-\pi}\text{Tr}[\boldsymbol{A}(k)]\,dk$ as a topological invariant to qualify its topological property. The matrix $\boldsymbol{A}(k)$ is expressed as $A(k)^{nm} = \langle\nu_n(k)|\partial_k|\nu_m(k)\rangle$, where n and m run over the degenerated band. It is found that the degenerated zero-energy band has a winding phase $\gamma_d = \pi$, and two isolated flat bands have $\gamma_{iso} = \pi/2$. The non-quantized bulk windings are consistent with that of the 1D AB cage, where the square of associated Hamiltonian can exhibit quantized topological exponents [21] (see Supplementary Note 4 for details). The square-root topological boundary states localize two strongly correlated anyons at the lattice edges. This localization persists even in the presence of disturbances or disorder. We expect that we can use this property to achieve robust anyon manipulations, which holds potential applications for future topological quantum computing.

3 Experimental simulation of anyonic topological flat bands by electric circuits

Realizing a topologically flat band induced by the quantum statistics of two anyons in a condensed matter system is highly challenging [48–50]. Generating effective anyon excitations in such systems is inherently difficult, requiring precise control and complex experimental conditions. In addition, our model includes the on-site interaction at both sublattices, NN interaction at "A" sublattice, single-particle hopping and direct two-anyon hopping. These requirements are currently beyond the reach of existing condensed matter systems. It has been demonstrated that the Fock space of a 1D few-body model exhibits a rigorous correspondence with a mapped high-dimensional lattice [53–55, 57]. Based on the similarity between circuit Laplacian and lattice Hamiltonian [58–69], electric circuits can be designed to construct the mapped 2D lattice. Figure 3(a) presents the schematic diagram of the circuit with $\theta = \pi$. Two circuit nodes connected by a capacitor C are regarded as an effective site in mapped 2D lattice, where voltages at two nodes can be formulated to achieve two voltage pseudospins $V_{\uparrow,\downarrow,(m,\alpha)(n,\beta)} = (V_{1,(m,\alpha)(n,\beta)} \pm V_{2,(m,\alpha)(n,\beta)})/\sqrt{2}$. Two capacitors C are used to link adjacent nodes without or with a cross to realize the effective hopping J or $Je^{\pm i\pi}$. Grounding capacitances C_V and C_U can implement the onsite interaction and NN interaction at "A" sublattice. Each node is also grounded by an inductor L. In this case, the circuit eigen-equation possesses the identical form with that of two anyons (See Supplementary Note 5 for the detailed derivation). The probability amplitude $C_{(m,\alpha)(n,\beta)}$ is mapped to the voltage pseudospin $V_{\downarrow,(m,\alpha)(n,\beta)}$. The eigen-energy is related to the eigen-frequency (f) of the circuit as $\varepsilon = f_0^2/f^2 - 10$ with $f_0 = 1/(2\pi\sqrt{CL})$. Two-anyon interactions are given by

024205-4

Xiaoqi Zhou, et al., Front. Phys. 20(2), 024205 (2025)
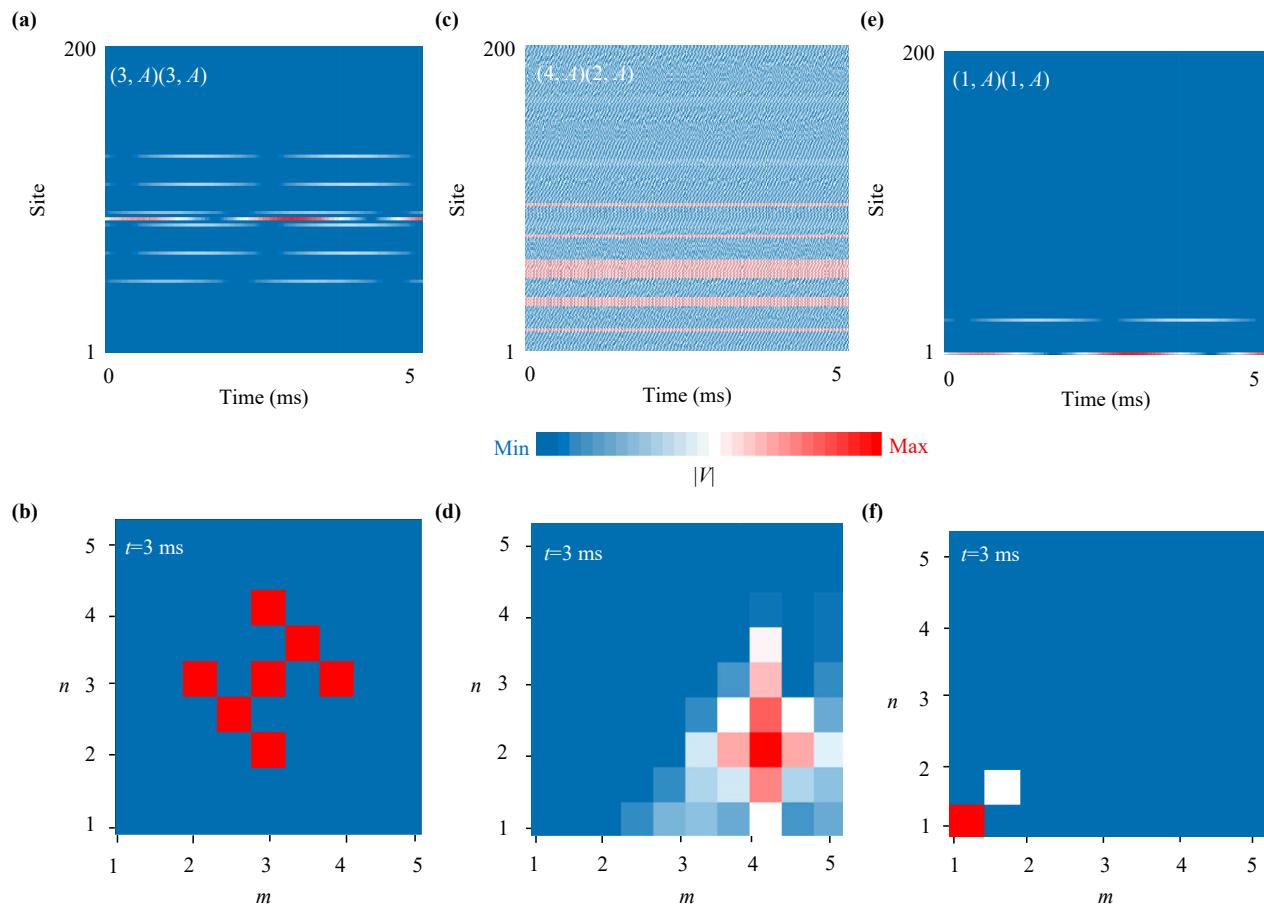
Fig. 3 Experimental simulations of quantum statistics-induced topological flat bands in electric circuits by impedance responses. **(a)** The schematic diagram of designed 2D circuit with $\theta = \pi$. Two circuit nodes connected by a capacitor C are regarded as an effective site in mapped 2D lattice, where voltages at two nodes can be formulated to achieve two voltage pseudospins $V_{\uparrow,\downarrow,(m,\alpha)(n,\beta)} = (V_{1,(m,\alpha)(n,\beta)} \pm V_{2,(m,\alpha)(n,\beta)})/\sqrt{2}$. Three insets illustrate the grounding of circuit structure. **(b)** Photograph images of the fabricated electric circuit near and far away from the diagonal. The corresponding parameters are set as $N = 5$, $C = 1$ nF, $C_p = 1.4$ nF, $C_U = 100$ nF, $C_V = 102.8$ nF and $L = 3.2$ μH. **(c, d)** Experimental results of impedance responses at two diagonal bulk nodes. **(e)** Green, orange and blue lines correspond to simulation results of impedance spectra at three diagonal circuit nodes. **(f, g)** Experimental and simulation results of impedance responses at an off-diagonal bulk node$(4, A), (2, A)$. **(h)** The measured impedance spectrum of an edge node at $(1, A), (1, A)$.

$U = (C_U + 2C_P)/C$ and $V = C_V/C$. The single-particle and two-anyon hoppings equal to $J = 1$ and $P = C_P/C$.

Two charts in Fig. 3(b) present photograph images of the fabricated electric circuit ($N = 5$) near and far away from the diagonal, where C, C_p, C_U, C_V and L are taken as 1 nF, 1.4 nF, 100 nF, 102.8 nF and 3.2 μH, respectively. Details on the sample fabrication are provided in Supplementary Note 6. Figure 3(c) presents the

measured impedance spectrum of a bulk node at $(3, A), (3, A)$. It is shown that two impedance peaks are observed at 0.262 MHz and 0.269 MHz, being matched to eigenenergies of two-anyon flatbands at $\varepsilon = 105.7$ and 100. The absence of an impedance peak related to the flat band at $\varepsilon = 102.8$ is rooted in the zero-valued probability amplitude of the corresponding eigenstate at $(n, A), (n, A)$ [shown in Fig. 2(f)]. Figure 3(d) presents

Fig. 4 Experimental simulations of quantum statistics-induced two-anyon flat-band localizations and topological edge states by voltage dynamics. **(a, c, e)** The experimental results of voltage dynamics by exciting a diagonal bulk node at $(3, A)(3, A)$ with $\omega = 1.691$ MHz, an off-diagonal bulk node at $(4, A)(2, A)$ with $\omega = 0.877$ MHz and an edge node at $(1, A)(1, A)$ with $\omega = 1.654$ MHz. **(b, d, f)** Distributions of voltage amplitudes at $t = 3$ ms related to (a), (c) and (e).

the measured impedance of the circuit node at $(3, B), (3, B)$. It is shown that there are three impedance peaks, corresponding to three two-anyon flat bands at $\varepsilon = 105.7$, 102.8 and 100. The associated simulation results are plotted in Fig. 3(e) by green and orange lines. A good consistence between simulations and measurements is obtained, and the larger width of measured impedance peaks results from the loss effect in the circuit sample (See Supplementary Note 7). Then, we measure the impedance spectrum for an off-diagonal circuit node at $(4, A), (2, A)$, as shown in Fig. 3(f). The corresponding simulation result is plotted in Fig. 3(g). It is found that there are many impedance peaks in the frequency range from 0.8 to 1.9 MHz, being matched to eigen-energies of two-anyon scattering states from $\varepsilon = 3.91$ to $\varepsilon = -3.91$.

To verify two-anyon topological edge states, we measure the impedance spectrum of an edge circuit node at $(1, A), (1, A)$, as shown in Fig. 3(h). The simulation result is presented by the blue line in Fig. 3(e). It is clearly shown that two impedance peaks at 0.263 MHz and 0.268 MHz are located in bandgaps between two-anyon flat bands, being consistent with eigenenergies of

two-anyon topological edge states. Because of the loss effect, the measured widths of impedance peaks are larger than that from simulations. Above results demonstrate that anyonic flat bands and topological edge states can be effectively emulated by our designed 2D electric circuits. In Supplementary Note 8, we further design electric circuits with varying values of effective statistical angles and calculate impedance responses to simulate the impact of effective statistical angle on the formation of anyonic topological flatbands in electric circuits.

Except for the impedance measurement, we further demonstrate the existence of anyonic flat bands by directly observing the flat-band-induced localization effect. Here, the input voltages are in the form of $V_{1,(m,\alpha)(n,\beta)} = V_0 e^{i\omega t}$, $V_{2,(m,\alpha)(n,\beta)} = -V_0 e^{i\omega t}$ to effectively excite the voltage pseudospin. Firstly, we input the voltage signal at $(3, A), (3, A)$ with $\omega = 1.691$ MHz (matched to $\varepsilon = 100$) to study the spatial localization induced by anyonic flat bands. The measured pseudospin voltages at all circuit nodes from 0 to 5 ms are plotted in Fig. 4(a). We can clearly see that the extremely large

voltage signal is concentrated on a few circuit nodes near the excitation point. The voltage profile at $t = 3$ ms is plotted in Fig. 4(b). It is shown that the voltage signal is concentrated at seven circuit nodes. Such a profile is consistent with the compact eigenmode of anyonic flatbands at $\varepsilon = 100$ [in Fig. 2(e)], showing the flat-band-induced spatial localization (or the anyonic caging effect). For comparison, we also measure the voltage evolution by exciting an off-diagonal circuit node $(4, A), (2, A)$ with $\omega = 0.877$ MHz (matched to a two-anyon scattering state), as shown in Fig. 4(c). In Fig. 4(d), we plot the spatial distribution of voltage amplitudes at $t = 3$ ms. It is found that the voltage signal rapidly spreads into the circuit sample.

Finally, we measure the voltage dynamics by exciting an edge circuit node at $(1, A), (1, A)$ with $\omega = 1.654$ MHz (matched to a two-anyon edge mode), as shown in Fig. 4(e). We also plot the distribution of voltage signal at $t = 3$ ms in Fig. 4(f). Owing to the existence of midgap topological edge states, the input voltage is strongly localized around the corner of the circuit sample. And, the input signal is concentrated at two boundary nodes $(1, A), (1, A)$ and $(1, B), (1, B)$, being matched to the distribution of a two-anyon topological edge state. Above experimental results are consistent with simulations in Supplementary Note 9. These phenomena can prove the simulation of two-anyon topological edge states induced by effective quantum statistics.

4 Conclusion

In conclusion, we have revealed that the emergence of topological flat bands can be driven purely by quantum statistics-induced synthetic gauge flux. Our study marks a significant departure from conventional flat-band topologies, which typically rely on complex hopping terms and external magnetic fields. Instead, we demonstrate that the anyonic flat-band topology arises entirely from the interference effects inherent in quantum statistics, effectively acting as synthetic magnetic fields. Furthermore, by mapping the eigenstates of two anyons onto electric circuit networks, we have successfully simulated the localization properties of anyonic flat bands and the corresponding square-root topological boundary states in an experimental setting. These findings not only offer a novel perspective on the role of quantum statistics in generating synthetic gauge fields but also provide a new framework for understanding and exploring topological phenomena in a wide range of physical systems. Our work opens up exciting possibilities for future research, including the exploration of other unconventional flat-band topologies and novel quantum phases driven by the interplay of strong interactions and quantum statistics. Additionally, the experimental real-

ization of these concepts in electric circuits paves the way for the development of innovative platforms for simulating complex quantum systems, potentially leading to new insights and applications in both fundamental physics and emerging technologies.

References

1. D. Leykam, A. Andreanov, and S. Flach, Artificial flat band systems: From lattice models to experiments, *Adv. Phys. X* 3(1), 1473052 (2018)

2. S. Mukherjee, A. Spracklen, D. Choudhury, N. Goldman, P. Öhberg, E. Andersson, and R. R. Thomson, Observation of a localized flat-band state in a photonic Lieb lattice, *Phys. Rev. Lett.* 114(24), 245504 (2015)

3. R. A. Vicencio, C. Cantillano, L. Morales-Inostroza, B. Real, C. Mejía-Cortés, S. Weimann, A. Szameit, and M. I. Molina, Observation of localized states in Lieb photonic lattices, *Phys. Rev. Lett.* 114(24), 245503 (2015)

4. M. R. Slot, T. S. Gardenier, P. H. Jacobse, G. C. P. van Miert, S. N. Kempkes, S. J. M. Zevenhuizen, C. M. Smith, D. Vanmaekelbergh, and I. Swart, Experimental realization and characterization of an electronic Lieb lattice, *Nat. Phys.* 13(7), 672 (2017)

5. P. Wang, Y. Zheng, X. Chen, C. Huang, Y. V. Kartashov, L. Torner, V. V. Konotop, and F. Ye, Localization and delocalization of light in photonic moiré lattices, *Nature* 577(7788), 42 (2020)

6. L. Balents, C. R. Dean, D. K. Efetov, and A. F. Young, Superconductivity and strong correlations in moiré flat bands, *Nat. Phys.* 16(7), 725 (2020)

7. Y. Choi, H. Kim, C. Lewandowski, Y. Peng, A. Thomson, R. Polski, Y. Zhang, K. Watanabe, T. Taniguchi, J. Alicea, and S. Nadj-Perge, Interaction-driven band flattening and correlated phases in twisted bilayer graphene, *Nat. Phys.* 17(12), 1375 (2021)

8. D. Călugăru, A. Chew, L. Elcoro, Y. Xu, N. Regnault, Z. D. Song, and B. A. Bernevig, General construction and topological classification of crystalline flat bands, *Nat. Phys.* 18(2), 185 (2022)

9. D. J. Thouless, M. Kohmoto, M. P. Nightingale, and M. den Nijs, Quantized Hall conductance in a two-dimensional periodic potential, *Phys. Rev. Lett.* 49(6), 405 (1982)

10. Y. Aharonov and D. Bohm, Significance of electromagnetic potential in the quantum theory, *Phys. Rev.* 115(3), 485 (1959)

Xiaoqi Zhou, et al., Front. Phys. 20(2), 024205 (2025)

024205-7

11. H. Aoki, M. Ando, and H. Matsumura, Hofstadter butterflies for flat bands, *Phys. Rev. B* 54(24), R17296 (1996)

12. J. Vidal, R. Mosseri, and B. Douçot, Aharonov–Bohm cages in two-dimensional structures, *Phys. Rev. Lett.* 81(26), 5888 (1998)

13. M. Creutz, End states, ladder compounds, and domain-wall fermions, *Phys. Rev. Lett.* 83(13), 2636 (1999)

14. C. C. Abilio, P. Butaud, T. Fournier, B. Pannetier, J. Vidal, S. Tedesco, and B. Dalzotto, Magnetic field induced localization in a two-dimensional superconducting wire network, *Phys. Rev. Lett.* 83(24), 5102 (1999)

15. S. Longhi, Aharonov–Bohm photonic cages in waveguide and coupled resonator lattices by synthetic magnetic fields, *Opt. Lett.* 39(20), 5892 (2014)

16. S. Mukherjee, M. Di Liberto, P. Öhberg, R. R. Thomson, and N. Goldman, Experimental observation of Aharonov–Bohm cages in photonic lattices, *Phys. Rev. Lett.* 121(7), 075502 (2018)

17. H. Wang, W. Zhang, H. Sun, and X. Zhang, Observation of inverse Anderson transitions in Aharonov–Bohm topolectrical circuits, *Phys. Rev. B* 106(10), 104203 (2022)

18. C. Jörg, G. Queraltó, M. Kremer, G. Pelegrí, J. Schulz, A. Szameit, G. von Freymann, J. Mompart, and V. Ahufinger, Artificial gauge field switching using orbital angular momentum modes in optical waveguides, *Light Sci. Appl.* 9(1), 150 (2020)

19. S. Li, Z. Y. Xue, M. Gong, and Y. Hu, Non-Abelian Aharonov–Bohm caging in photonic lattices, *Phys. Rev. A* 102(2), 023524 (2020)

20. H. Li, Z. Dong, S. Longhi, Q. Liang, D. Xie, and B. Yan, Aharonov–Bohm Caging and inverse Anderson transition in ultracold atoms, *Phys. Rev. Lett.* 129(22), 220403 (2022)

21. M. Kremer, I. Petrides, E. Meyer, M. Heinrich, O. Zilberberg, and A. Szameit, A square-root topological insulator with non-quantized indices realized with photonic Aharonov–Bohm cages, *Nat. Commun.* 11(1), 907 (2020)

22. J. Vidal, B. Douçot, R. Mosseri, and P. Butaud, Interaction-induced delocalization for two particles in a periodic potential, *Phys. Rev. Lett.* 85(18), 3906 (2000)

23. C. E. Creffield and G. Platero, Coherent control of interacting particles using dynamical and Aharonov-Bohm Phases, *Phys. Rev. Lett.* 105(8), 086804 (2010)

24. J. G. Martinez, C. S. Chiu, B. M. Smitham, and A. A. Houck, Flat-band localization and interaction-induced delocalization of photons, *Sci. Adv.* 9(50), eadj7195 (2023)

25. G. Möller and N. R. Cooper, Correlated phases of bosons in the flat lowest band of the dice lattice, *Phys. Rev. Lett.* 108(4), 045306 (2012)

26. C. Cartwright, G. De Chiara, and M. Rizzi, Rhombi-chain Bose–Hubbard model: Geometric frustration and interactions, *Phys. Rev. B* 98(18), 184508 (2018)

27. G. Pelegrí, A. M. Marques, V. Ahufinger, J. Mompart, and R. G. Dias, Interaction-induced topological properties of two bosons in flat-band systems, *Phys. Rev. Res.* 2(3), 033267 (2020)

28. Y. Kuno, T. Mizoguchi, and Y. Hatsugai, Interaction-induced doublons and embedded topological subspace in a complete flat-band system, *Phys. Rev. A* 102(6), 063325 (2020)

29. M. Di Liberto, S. Mukherjee, and N. Goldman, Nonlinear dynamics of Aharonov–Bohm cages, *Phys. Rev. A* 100(4), 043829 (2019)

30. J. Zurita, C. E. Creffield, and G. Platero, Topology and interactions in the photonic Creutz and Creutz–Hubbard ladders, *Adv. Quantum Technol.* 3(2), 1900105 (2020)

31. C. Danieli, A. Andreanov, T. Mithun, and S. Flach, Quantum caging in interacting many-body all-bands-flat lattices, *Phys. Rev. B* 104(8), 085132 (2021)

32. E. Nicolau, A. M. Marques, R. G. Dias, J. Mompart, and V. Ahufinger, Many-body Aharonov–Bohm caging in a lattice of rings, *Phys. Rev. A* 107(2), 023305 (2023)

33. J. M. Leinaas and J. Myrheim, On the theory of identical particles, *Nuovo Cimento B* 37(1), 1 (1977)

34. G. A. Goldin, R. Menikoff, and D. H. Sharp, Particle statistics from induced representations of a local current group, *J. Math. Phys.* 21(4), 650 (1980)

35. G. A. Goldin, R. Menikoff, and D. H. Sharp, Representations of a local current algebra in nonsimply connected space and the Aharonov–Bohm effect, *J. Math. Phys.* 22(8), 1664 (1981)

36. F. Wilczek, Magnetic flux, angular momentum, and statistics, *Phys. Rev. Lett.* 48(17), 1144 (1982)

37. F. Wilczek, Quantum mechanics of fractional-spin particles, *Phys. Rev. Lett.* 49(14), 957 (1982)

38. G. S. Canright and S. M. Girvin, Fractional statistics: Quantum possibilities in two dimensions, *Science* 247(4947), 1197 (1990)

39. F. D. M. Haldane, "Fractional statistics" in arbitrary dimensions: A generalization of the Pauli principle, *Phys. Rev. Lett.* 67(8), 937 (1991)

40. A. Kundu, Exact solution of double δ function Bose gas through an interacting anyon gas, *Phys. Rev. Lett.* 83(7), 1275 (1999)

41. A. Kitaev, Anyons in an exactly solved model and beyond, *Ann. Phys.* 321(1), 2 (2006)

42. T. Keilmann, S. Lanzmich, I. McCulloch, and M. Roncaglia, Statistically induced phase transitions and anyons in 1D optical lattices, *Nat. Commun.* 2(1), 361 (2011)

43. H. Bartolomei, M. Kumar, R. Bisognin, A. Marguerite, J. M. Berroir, E. Bocquillon, B. Plaçais, A. Cavanna, Q. Dong, U. Gennser, Y. Jin, and G. Fève, Fractional statistics in anyon collisions, *Science* 368(6487), 173 (2020)

44. J. Nakamura, S. Liang, G. C. Gardner, and M. J. Manfra, Direct observation of anyonic braiding statistics, *Nat. Phys.* 16(9), 931 (2020)

45. M. T. Batchelor, X. W. Guan, and N. Oelkers, One-dimensional interacting anyon gas: Low-energy properties and Haldane exclusion statistics, *Phys. Rev. Lett.* 96(21), 210402 (2006)

46. E. Fradkin, Jordan–Wigner transformation for quantum-spin systems in two dimensions and fractional statistics, *Phys. Rev. Lett.* 63(3), 322 (1989)

47. S. Longhi and G. Della Valle, Anyonic Bloch oscillations, *Phys. Rev. B* 85(16), 165144 (2012)

024205-8

Xiaoqi Zhou, et al., Front. Phys. 20(2), 024205 (2025)

48. C. Nayak, S. H. Simon, A. Stern, M. Freedman, and S. Das Sarma, Non-Abelian anyons and topological quantum computation, *Rev. Mod. Phys.* 80(3), 1083 (2008)

49. T. Wang, X. Cheng, G. Zhang, K. Yuan, H. Chen, and L. Wang, Spin-gapless semiconductors for future spintronics and electronics, *Phys. Rep.* 888, 1 (2020)

50. T. Yang, H. Wang, P. Li, T. Wang, X. Cheng, H. Wang, and G. Zhang, Topological nodal-point phononic systems, *Matter* 7(2), 320 (2024)

51. F. Liu, J. R. Garrison, D. L. Deng, Z. X. Gong, and A. V. Gorshkov, Asymmetric particle transport and light-cone dynamics induced by anyonic statistics, *Phys. Rev. Lett.* 121(25), 250404 (2018)

52. Y. Qin, C. H. Lee, and L. Li, Dynamical suppression of many-body non-Hermitian skin effect in anyonic systems, arXiv: 2405.12288 (2024)

53. W. Zhang, H. Yuan, H. Wang, F. Di, N. Sun, X. Zheng, H. Sun, and X. Zhang, Observation of Bloch oscillations dominated by effective anyonic particle statistics, *Nat. Commun.* 13(1), 2392 (2022)

54. W. Zhang, Q. Long, H. Sun, and X. Zhang, Anyonic bound states in the continuum, *Commun. Phys.* 6(1), 139 (2023)

55. N. A. Olekhno, A. D. Rozenblit, A. A. Stepanenko, A. A. Dmitriev, D. A. Bobylev, and M. A. Gorlach, Topological transitions driven by quantum statistics and their electrical circuit emulation, *Phys. Rev. B* 105(20), 205113 (2022)

56. V. Brosco, L. Pilozzi, and C. Conti, Two-flux tunable Aharonov–Bohm effect in a photonic lattice, *Phys. Rev. B* 104(2), 024306 (2021)

57. J. M. Koh, T. Tai, and C. H. Lee, Realization of higher-order topological lattices on a quantum computer, *Nat. Commun.* 15(1), 5807 (2024)

58. J. Ningyuan, C. Owens, A. Sommer, D. Schuster, and J. Simon, Time- and site-resolved dynamics in a topological circuit, *Phys. Rev. X* 5(2), 021031 (2015)

59. V. V. Albert, L. I. Glazman, and L. Jiang, Topological properties of linear circuit lattices, *Phys. Rev. Lett.* 114(17), 173902 (2015)

60. C. H. Lee, S. Imhof, C. Berger, F. Bayer, J. Brehm, L. W. Molenkamp, T. Kiessling, and R. Thomale, Topolectrical circuits, *Commun. Phys.* 1(1), 39 (2018)

61. S. Imhof, C. Berger, F. Bayer, J. Brehm, L. W. Molenkamp, T. Kiessling, F. Schindler, C. H. Lee, M. Greiter, T. Neupert, and R. Thomale, Topolectrical-circuit realization of topological corner modes, *Nat. Phys.* 14(9), 925 (2018)

62. Y. Wang, H. M. Price, B. Zhang, and Y. D. Chong, Circuit implementation of a four-dimensional topological insulator, *Nat. Commun.* 11(1), 2356 (2020)

63. T. Helbig, T. Hofmann, S. Imhof, M. Abdelghany, T. Kiessling, L. W. Molenkamp, C. H. Lee, A. Szameit, M. Greiter, and R. Thomale, Generalized bulk–boundary correspondence in non-Hermitian topolectrical circuits, *Nat. Phys.* 16(7), 747 (2020)

64. N. A. Olekhno, E. I. Kretov, A. A. Stepanenko, P. A. Ivanova, V. V. Yaroshenko, E. M. Puhtina, D. S. Filonov, B. Cappello, L. Matekovits, and M. A. Gorlach, Topological edge states of interacting photon pairs realized in a topolectrical circuit, *Nat. Commun.* 11(1), 1436 (2020)

65. W. Zhang, D. Zou, Q. Pei, W. He, J. Bao, H. Sun, and X. Zhang, Experimental observation of higher-order topological Anderson insulators, *Phys. Rev. Lett.* 126(14), 146802 (2021)

66. J. Wu, Z. Wang, Y. Biao, F. Fei, S. Zhang, Z. Yin, Y. Hu, Z. Song, T. Wu, F. Song, and R. Yu, Non-Abelian gauge fields in circuit systems, *Nat. Electron.* 5(10), 635 (2022)

67. L. Song, H. Yang, Y. Cao, and P. Yan, Square-root higher-order Weyl semimetals, *Nat. Commun.* 13(1), 5601 (2022)

68. W. Zhang, H. Yuan, N. Sun, H. Sun, and X. Zhang, Observation of novel topological states in hyperbolic lattices, *Nat. Commun.* 13(1), 2937 (2022)

69. W. Zhang, F. Di, X. Zheng, H. Sun, and X. Zhang, Hyperbolic band topology with non-trivial second Chern numbers, *Nat. Commun.* 14(1), 1083 (2023)

Xiaoqi Zhou, et al., Front. Phys. 20(2), 024205 (2025)

024205-9